Geophys. J. Int. (2001) **147,** 415–427

A modelling study of vertical surface displacements at convergent plate margins

Susanne J. H. Buiter,* Rob Govers and M. J. R. Wortel

Vening Meinesz Research School of Geodynamics, Utrecht University, Budapestlaan 4, 3584 *CD Utrecht, the Netherlands*

Accepted 2001 June 25. Received 2001 June 21; in original form 2000 March 20

SUMMARY

During the evolution of a subduction zone system, variations are likely to occur in, for example, surface plate velocities and buoyancy of the subducting lithosphere. We quantify vertical surface displacements at convergent plate margins resulting from such imposed variations. For this purpose we use a 2-D numerical model in which the lithospheric plates have an effective elastic thickness. We first define a model in which the subducting plate is driven by its negative buoyancy and a velocity at its surface side boundary. Its equilibrium topography (after around 2 Myr) is the reference level for examination of surface displacements resulting from variations in buoyancy, velocity of the surface plates, friction along the interplate contact and subduction zone roll-back. We find that a decrease (increase) in buoyancy of the subducting material leads to a deepening (uplift) of the plate margins. An increase in friction along the subduction fault deepens the overriding plate margin. Subduction zone roll-back due to sinking of the negatively buoyant subducting plate induces subsidence of the overriding plate margin. This subsidence is reduced when roll-back takes place in a land-locked basin setting. Trench retreat forced by the motion of the overriding plate is characterized by higher topography of the overriding plate margin than the case of retreat due to the sinking of the negatively buoyant slab. In the first case in-plane stress in the back-arc region is compressive while it is tensional for roll-back due to the sinking of the slab. We conclude that vertical surface displacements during ongoing subduction may reach a magnitude of a few kilometres on the overriding and subducting plate margins.

Key words: active margin, finite element method, subduction, subsidence, uplift.

1 INTRODUCTION

1.1 Aims and approach

Observations show that vertical displacements of the Earth's surface near convergent plate margins may reach magnitudes of the order of hundreds of metres to several kilometres (e.g. Audley-Charles 1986; Lundberg & Dorsey 1988; Westaway 1993; Doglioni 1993). These displacements may be caused by various processes that are related to plate convergence. For example, the initiation of subduction may induce subsidence of the overriding plate of the order of a few kilometres (Gurnis 1992), while the termination of subduction will probably lead to uplift (Chatelain *et al.* 1992; Westaway 1993). In this study, we concentrate on vertical displacements during the phase of ongoing subduction between the first (initiation) and final (termination) stages of a subduction zone system. The aim of our study is to quantify vertical surface displacements near convergent plate margins resulting from variations in a subduction zone system on a timescale of a few million years. It is not our purpose to reproduce the characteristics of a specific subduction zone, but instead to predict in a more general sense which observable effects may be expected from imposed variations in a subduction zone system. Such variations are more likely to be a rule than an exception. For example, with time there will be changes in age of the subducting lithosphere, in velocities of the lithospheric plates due to larger-scale plate reorganizations and in mantle flow patterns. We study the effect of such variations on the flexural behaviour of the lithospheric plates involved on a regional scale. Since subduction occurs at time and depth scales that limit direct observations, we make use of model experiments.

We present a 2-D numerical method for modelling subduction zone dynamics on a timescale of a few million years with a lithosphere model in which the asthenosphere is not explicitly included. The lithospheric plates in the model are elastic, which leads to the use of an effective thickness. Plates

* Now at: Geological Institute, University of Bern, Baltzerstrasse 1, 3012 Bern, Switzerland. E-mail: susanne@mpi.unibe.ch

with an effective elastic thickness adequately simulate the surface deflections at a subduction zone (e.g. Watts & Talwani 1974; Caldwell *et al.* 1976). Our choice of a numerical elastic model to study subduction zone dynamics is motivated by a number of considerations. First, the geometry of a subducting plate at the trench may well be approximated by the bending of an elastic plate. We recognize that the whole lithosphere will not behave elastically on geological timescales and that bending will be accompanied by inelastic deformation (Chapple & Forsyth 1979; Conrad & Hager 1999). This aspect is incorporated in our model by using an effective thickness (which is smaller than the lithospheric thickness). Second, in purely viscous models subducting slabs tend to steepen with time and a non-vertical slab may be obtained by introducing additional factors such as trench migration or horizontal mantle flow (Christensen 1996; Becker *et al.* 1999). In elastic or viscoelastic models shallow slab dip angles result without the need to invoke these factors (Hassani *et al.* 1997). Third, the development of surface topography is an integral part of the method in mechanical models. In viscous models (e.g. Zhong & Gurnis 1994; Gurnis *et al.* 1996) dynamic topography is derived from the normal stress at the surface of the model. The advantage of numerical experiments in comparison with analogue models is a larger freedom in choice of material parameters, while stress and topography can be determined at all stages of the experiment.

1.2 Relation to previous studies

In the following sections we discuss viscoelastic models of subduction zone dynamics. Our limitation to this category of models is motivated partly by the importance we attribute to elasticity in subduction models and partly by the work of Gurnis *et al.* (1996) who show that topography near a convergent plate margin is overall remarkably similar for viscous and viscoelastic models. The viscoelastic models have a wider and deeper trench, and a more prominent forebulge.

Previous viscoelastic models of subduction can be divided into short- and long-term simulations. The first category involves models used to study the instantaneous reaction of a subduction zone system to the application of loads or to changes in the subduction process. An example is the approach taken by Whittaker *et al.* (1992), who applied the density difference between the subducting plate and the surrounding mantle (slab pull) and calculated the resulting intraplate stresses and plate boundary forces. They show that the interplate contact needs to be (partly) unlocked in order to enable back-arc stretching. Extending this approach, Giunchi *et al.* (1996) matched present-day horizontal and vertical surface velocities for the southern Tyrrhenian Sea (Italy) with a viscoelastic model (see also Negredo *et al.* 1997). The timescale of these simulations is of the order of 200 kyr. The modelling approach used in these studies has its limitations in cases where surface displacements are examined that are due to forcings on geological timescales, such as subduction. In the above examples, the model evolution starts with an already bent subducted lithosphere in which flexural bending stresses are not taken into account. In reality, subducting lithosphere bends at the trench and unbends at depth. To achieve unbending on longer timescales, bending stresses have to be included in (visco)elastic models. These can be incorporated by appropriate initialization and/or integration over a sufficiently long time (of the order of millions of years).

Models of subduction on longer timescales have been used to examine convergent plate margin topography, mostly not with the aim of determining variations in this topography. Ongoing subduction has been modelled with a viscoelastic rheology by Gurnis *et al.* (1996), who examine trench topography starting from a pre-defined subduction geometry and integrating the model for 5 Myr. They find that topography depends on lithospheric viscosity, subduction fault dip angle and slab dip angle, but the effects were not all quantified. Toth & Gurnis (1998) show that active margin topography depends on the depth of slab penetration, the age of the slab, mantle viscosity and the dip angle of the subduction fault. They show changes in surface topography of up to around 3 km. Since their study focuses on the initiation of subduction, the calculated topography is the result of all processes active since the start of subduction and has not yet reached equilibrium at the time the model simulations are compared with one another. In contrast, we examine surface effects resulting from variations in a fully developed subduction zone that is in steady state prior to the imposed change. Hassani *et al.* (1997) simulate subduction initiation, continued subduction and subduction zone roll-back with a (visco)elastic model. Their results are in good agreement with the analogue models of Shemenda (1993). Their simulations show that variations in surface topography of several kilometres may result from changes in the density contrast between the subducting plate and the mantle or from subduction zone roll-back. Our modelling approach is similar to the method of Hassani *et al.* (1997), for example, in the use of an effective elastic thickness and in simulating the asthenosphere–lithosphere interaction through boundary conditions. The main differences lie (i) in the initiation phase, since we do not model subduction initiation but initialize our model trough bending of a horizontal plate, and (ii) in the way we include the effects of subducted lithosphere outside our model domain.

Our focus lies in the examination of vertical surface displacements resulting from the following processes: variations in buoyancy of the subducting plate, velocity of the surface plates, friction along the interplate contact, and slab retrograde motion. We present the results of the modelling of subduction zone roll-back caused by two different driving mechanisms: outward trench migration caused by the sinking of the negatively buoyant subducting plate (Elsasser 1971) or forced by the motion of the overriding plate (Cross & Pilger 1982). Processes such as underplating, magmatism, erosion, sedimentation and thrusting are not included in our analysis.

2 MODELLING METHOD

2.1 Equations and rheology

To study the effects of subduction on surface displacements near convergent plate margins, we use a 2-D numerical model that is on the scale of the whole lithosphere. The mechanical evolution of lithosphere on geological timescales is governed by the equilibrium equation

$$\nabla \cdot \bar{\bar{\sigma}} + \rho \bar{g} = 0 \qquad + \text{ boundary conditions}, \tag{1}$$

where $\bar{\bar{\sigma}}$ is the stress tensor, ρ is the mass density and $\bar{g}$ is the gravitational acceleration. This equation is solved using the finite element code TECTON, which was originally written by Melosh & Raefsky (1980) (see also Melosh & Raefsky 1983;

Melosh & Williams 1989). In our models, the body force term ($\rho\bar{g}$) is replaced by boundary conditions on the model sides. These are discussed below (see Section 2.4). The implication of this approach is that the effects of lateral density variations inside the model plates are neglected. We account for the effects of large deformations by using the formulation of Wallace & Melosh (1994). We assume that no deformation occurs perpendicular to the plane of our model and, therefore, the plane strain approximation is adopted. The convention is used that compression is negative and tension is positive.

On geological timescales, the response of the lithosphere to internal or external forcing is governed by a depth-dependent rheology that includes elastic, plastic and viscous behaviour. In our study we quantify surface deflections induced by changes in a subduction zone system. To mimic the bending of thick lithosphere with a realistic depth-dependent rheology, we use model plates with an effective elastic thickness (e.g. Watts & Talwani 1974; Caldwell *et al.* 1976). We note that magnitudes of stresses and strains as predicted by our elastic model differ from those for a depth-dependent rheology. It is, however, intrinsic to the deployment of the concept of a plate with an effective elastic thickness that bending moments in the elastic model are identical to those for a realistic rheology and lithospheric thickness. In spite of differences in the distribution of stresses, this means that surface deflections as predicted by our models are identical to those for a depth-dependent rheology. We use one fixed value for the effective elastic thickness of the lithosphere. If the evolution of a specific geological region were simulated, this value would have to be varied or constrained by independent information, e.g. thermal and age data.

In our models of subduction zone roll-back, we introduce a local zone of weakness in the overriding plate with the purpose of localizing extension and facilitating the formation of a back-arc basin. The weak zone is simulated by a zone of lower viscosity in the same manner as in Hassani *et al.* (1997). This part of the model has a Newtonian viscoelastic rheology.

2.2 Geometry

Our model consists of a subducting and an overriding lithospheric plate (Fig. 1). The asthenosphere is not explicitly included in the model domain. Our considerations for this approach are the following. Subduction models that either incorporate the asthenosphere (e.g. Gurnis *et al.* 1996) or do not incorporate it (e.g. Hassani *et al.* 1997) all require a description of the physical situation beyond the model domain in order to be able to define boundary conditions on the model domain sides. In both cases one has to be aware that the chosen boundary conditions can affect the processes under investigation. For lithosphere models that do incorporate the asthenosphere, the choice of boundary conditions on the sides (e.g. rigid or in/outflow) or bottom (e.g. permeable or impermeable) of the computational domain influence slab behaviour as shown by Davies (1995) and Christensen (1996), respectively. Also, rigid side boundaries can affect slab roll-back, since asthenospheric flow in the direction of slab translation is limited. The above considerations imply that for models in which the asthenosphere is included the effect of the chosen boundary conditions on subduction zone behaviour would have to be investigated and clearly specified. We have chosen to represent the effects of the asthenosphere on the lithosphere through pressure boundary conditions that act directly on the model lithosphere. These are discussed in Section 2.4.3. A limitation of such a model without asthenosphere is clearly that the lithosphere–asthenosphere interaction is simulated.

Our simulations are aimed at examining the response to imposed changes of a fully developed subduction zone, i.e. with a long slab. The slab in our model is relatively short and initially extends to 90 km depth (Fig. 1). Below we discuss the boundary conditions acting on the model slab end that represent a slab extending deeper into the mantle (Section 2.4).

In our model, the contact between the subducting and the overriding plate is a slippery fault (Melosh & Williams 1989), which can deform and migrate. We have modified the slippery fault formulation in such a way that the fault slip is locally always parallel to the fault geometry. Initially, the subduction fault is curved and it follows the geometry of the subducting plate. The coefficient of friction on the fault is defined as $\mu = |\tau| / |\sigma_n|$ (where τ is the shear stress and σ_n is the normal stress on the plate contact including gravitational pressure).

The model domain has been divided into 1557 isoparametric triangles built from 959 nodes (Fig. 1). The models are integrated with 1000 yr time-steps over several million years, until a total displacement in the range of 50–150 km is achieved. We have performed convergence tests with a finer mesh (2953 elements) or smaller a time-step (500 yr) that confirmed that our results have converged.

2.3 Consistent initial geometry and pre-stresses

Since the initiation of subduction is not the focus of our study, we avoid the implementation of a subduction initiation phase and start our models from the geometry of an already bent subducting plate. Because we are interested in subduction on longer timescales this approach requires that bending pre-stresses are incorporated in a manner that is consistent with the initial geometry. These pre-stresses allow for unbending at depth of subducted lithosphere in the case of an elastic rheology. To compute bending stresses that are dynamically consistent with a subduction geometry, we include an initialization phase in the modelling. A horizontal plate is flexed by stresses at one plate end while the other end is held fixed. We have verified that

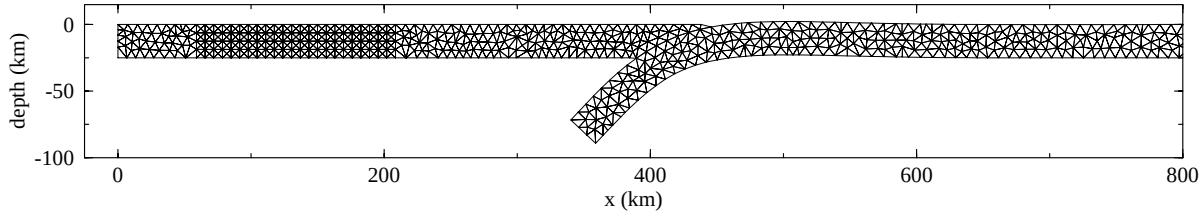

Figure 1. Finite element grid. The subducting plate initially extends to 1226 km in the horizontal direction and is not completely shown here. Discretization in the subducting plate is slightly coarser towards the right edge.

this approach leads to a geometry that agrees with existing subduction zone geometries as defined by Benioff zones. The overriding lithosphere is subsequently added to the subducted plate to complete our initial model (Figs 1 and 2).

We remesh the grid after the initialization phase to avoid deformations that are too large. All boundary conditions, rheological parameters and stresses are mapped onto the new grid and the calculations are restarted. We are aware that remeshing may introduce inaccuracies in the calculations. To minimize these, we enforce equilibrium between nodal forces and element stresses by calculating the initial nodal forces on the new grid from the stresses. The model has to be integrated for a sufficient amount of time to ensure that the effects of the initialization have disappeared and equilibrium between geometry, stresses and boundary conditions is established. We show (Section 3) that for our models this is achieved after approximately 2 Myr.

2.4 Boundary conditions

2.4.1 Horizontal plates

Viewed on a large scale, plate motions are in large part driven by slab pull and ridge push forces. These forces are counteracted by resistive forces such as plate contact resistance and viscous resistance exerted by the mantle on the subducting slab. With our model we represent only part of this system. We include the net effect of forces outside the model domain

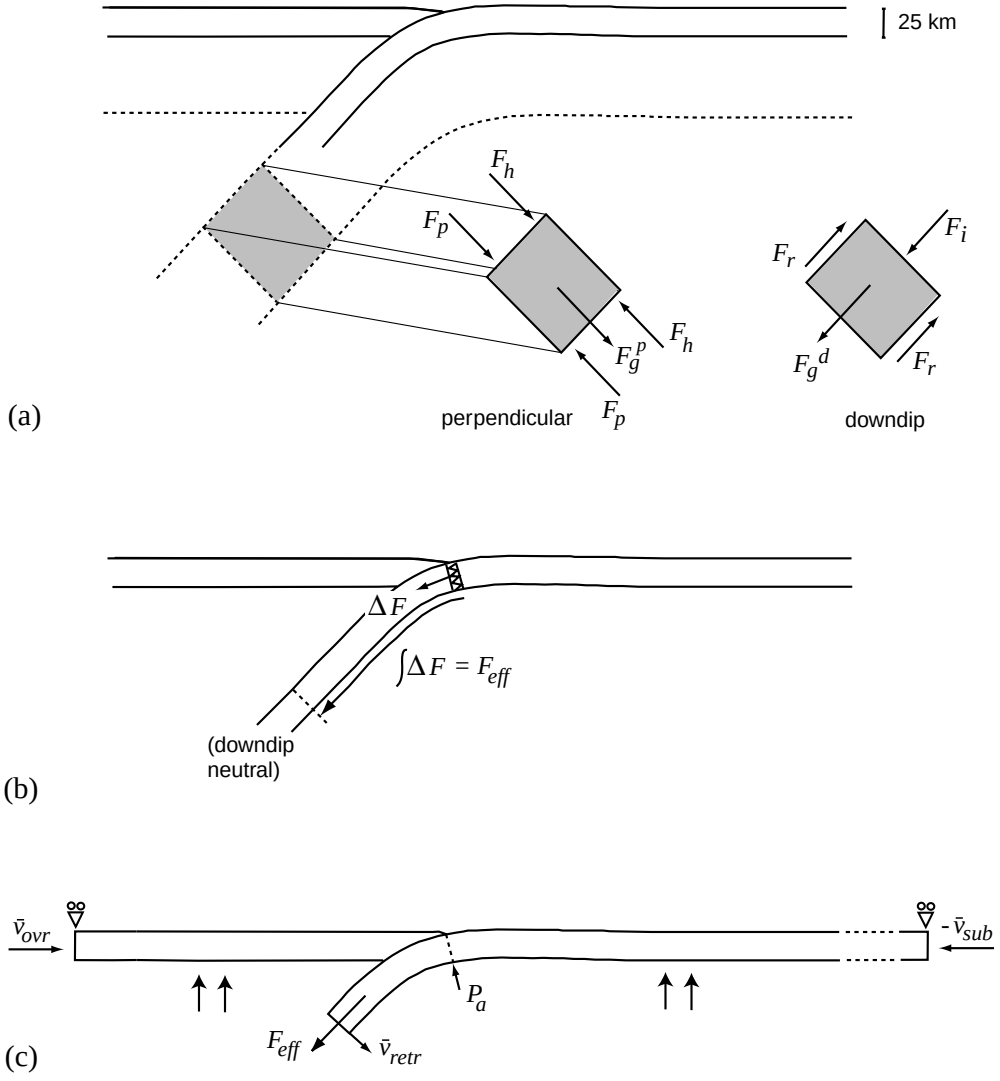

Figure 2. (a) The behaviour of the thick lithosphere of the overriding and the subducting plates (dotted line) is approximated in the model by using plates with an effective elastic thickness (solid line). Forces acting on part of the subducting plate are indicated: F_g slab pull, F_h hydrostatic restoring force, F_p force due to pressure differences, F_i ridge push and F_r resistive force. (b) Subduction of a new slab segment at the trench (denoted with zigzags) generates a force increment ΔF. Integration of the force increments along the slab from the trench to the depth where the slab is considered neutral in a forcing sense (see Section 2.4.3) gives the total effective pull force $F_{\rm eff}$. (c) Schematic illustration of the model and general boundary conditions. The subducting plate experiences an effective pull force ($F_{\rm eff}$) oriented down the dip of the slab. Subduction zone roll-back is simulated through a slab-normal velocity ($\bar{v}_{\rm retr}$) applied at the model slab end. The right-hand-side boundary of the subducting plate and the left hand side of the overriding plate are held fixed laterally or move with a prescribed velocity. The orientation and magnitudes of the velocities can change. The rollers at the top left and right corners indicate that the corners are not allowed to move vertically. The black arrows indicate the hydrostatic pressure that is exerted by the asthenosphere on the lithospheric plates. See text (Section 2.4.3) for the definition of $P_{\rm a}$.

through velocity boundary conditions at the left and right sides of the surface plates (Fig. 2c), since these are observationally constrained. We assume that (driving or resistive) basal drag is absent in our model domain.

2.4.2 *Subduction forcing*

Subducting lithosphere experiences a slab pull force due to the density difference with the surrounding mantle. This density difference is reduced by thermal assimilation as slab material moves further down into the mantle. The motion of the slab in the mantle gives rise to frictional resistive forces that act to reduce the effect of slab pull. The result is an effective pull force. The subducted slab in our initial model (Fig. 2) corresponds to an effective pull force $F^0_{\rm eff}$ of 2.4×10^{13} N m^{-1} directed along the dip of the slab. As new slab segments subduct, they generate a force increment ΔF^0. This force increment also consists of a driving contribution due to the density difference with the surrounding material and a counteractive contribution formed by resistive forces. Integration of the force increments along the slab results in the effective pull force $F^0_{\rm eff}$ (Fig. 2b). Details concerning the determination of the magnitude of the pull force and the manner in which the force is applied in the numerical model are given in Appendix A.

The stress solution of the equilibrium equations (1) represents mechanical equilibrium between model geometry and forces acting in and on the model. Imposing a force on a constrained elastic body results in a solution of stress and geometry that does not change with time. In our model, however, slab pull is not a static quantity. With time, new segments of the subducting plate move down into the mantle and their density difference with the surrounding mantle material contributes to the slab pull force.

2.4.3 *Viscous asthenosphere*

The asthenosphere is included in our models through boundary conditions that simulate its interaction with the lithospheric plates. In our view, the main contributions to this interaction are (i) hydrostatic pressure, (ii) dynamic pressures and (iii) viscous resistance. These are discussed below.

(i) *Hydrostatic pressure*. At the viscosity of the asthenosphere (of the order of 10^{21} Pa s), the relaxation time of a viscoelastic (Maxwell) body is of the order of a few thousand years. This means that the asthenosphere can be considered to be in hydrostatic equilibrium on geological timescales. The pressure increases linearly with depth at a rate $\Delta p=\rho_{\rm a}g\Delta z$, where p is the pressure, $\rho_{\rm a}$ is the density of the asthenosphere and z is depth. In this expression we neglect the compressibility of the asthenospheric material, which would lead to only a small difference in the pressures in the shallow upper mantle, e.g. 3 per cent at 200 km depth (see Hassani *et al.* (1997) for a formulation that includes asthenospheric compressibility). The hydrostatic pressure effectively acts as a restoring pressure that opposes vertical displacement of lithospheric plates at the Earth's surface. In our numerical model, a hydrostatic pressure acts on all lithospheric boundaries that are in contact with the asthenosphere.

Once material is fully subducted, the hydrostatic pressure acts on both the upper and the lower sides of the subducting plate (Fig. 2a). If it is assumed that density does not change strongly with depth [which is a reasonable approximation for the upper mantle depths in our models (e.g. PREM, Dziewonski & Anderson 1981)], a vertical displacement leads to the same pressure increments on the upper and lower sides of the plate, when viewed in cross-section. For the subducting plate, therefore, we take these forces out of the system of equations. We do the same for the part of the subducting plate that is still in contact with the overriding plate. We assume, therefore, that the pressure exerted by the overriding plate on the subducting plate is hydrostatic. In our models, hydrostatic pressure increments due to slab displacement are considered to be in balance along the part of the slab below the line indicated by model parameter $P_{\rm a}$ in Fig. 2(c). In all simulations except two (models 5 and 10), this line is determined by the (perpendicular downward projection of the) point of contact of the overriding plate with the subducting plate at the surface. The location of $P_{\rm a}$ will, therefore, change during model evolution in the case of trench migration. The balance in hydrostatic pressures near the contact with the overriding plate may be affected by changes in the density of the overriding plate and changes in the amount of material lying on the subducting plate near the trench. These effects may be incorporated through variation of the location of $P_{\rm a}$. A larger accretionary wedge, for example, will exert a downward pressure over a larger area and shift $P_{\rm a}$ oceanwards.

(ii) *Dynamic pressures*. During subduction, motions of the lithospheric plates induce flow of mantle material on both sides of the subducting lithosphere. This corner flow exerts a lifting pressure on the subducting slab, which may contribute to maintaining a non-vertical slab dip. It has been shown (Stevenson & Turner 1977; Tovish *et al.* 1978; Dvorkin *et al.* 1993) that the moments due to corner flow and the negative buoyancy of the slab can be in equilibrium. In our models, the orientation of the subducted slab is determined by the balance between forces that act in a direction normal to the slab (Fig. 2a). In the case of steady non-migrating subduction, we assume that the slab-normal component of slab pull and dynamic (corner flow) pressures balance each other. Therefore, these forces do not contribute to slab dip changes. The case of slab retrograde motion is discussed below (Section 2.4.4). For the region where the subducting plate is still in contact with the overriding plate and has not yet straightened out, we assume that the slab-normal component of slab pull is balanced by dynamic pressures other than corner flow. Such dynamic pressures could, for example, arise from horizontal density differences or from dynamic bending moments induced in the overriding plate during the phase of subduction initiation.

(iii) *Viscous resistance.* There is no seismological evidence of thickening or thinning of subducted slabs during their descent in the shallow upper mantle (disregarding slab detachment). The inference is that slabs do not accelerate or slow down following subduction. As it moves in the mantle a subducting plate will experience a viscous resistance. This frictional drag exerted by the mantle on the sides and leading edge of the subducting lithosphere acts to reduce the effect of the along-dip component of slab pull. In our model, we assume that once the slab has straightened out, the along-dip component of slab pull is balanced by viscous resistive forces and internal stresses (due to the plate segment being attached to the rest of the subducting plate). The slab-parallel velocity remains constant with time, that is, the slab has reached its terminal velocity (e.g. Marton *et al.* 1999). When the slab has not yet straightened

out, the along-dip component of slab pull is not completely balanced by other forces. This leads to the aforementioned effective force increments ΔF.

2.4.4 Roll-back

We assume that retrograde motion of the subducting plate can occur when the slab-normal component of slab pull and dynamic mantle pressures are not completely in balance. This can take place, for example, in the case of a narrow subduction zone (narrow in the along-trench direction), a short subducting slab or a discontinuous slab, whence mantle material can more easily flow around the subducting plate (Dvorkin *et al.* 1993). In this way the building up of dynamic pressures is reduced and retrograde motion of the slab is facilitated. We examine the case where roll-back is driven by out-of-balance pressures along the part of the slab that has straightened out. The case of roll-back driven by pressure differences along the part of the subducting plate that is still in contact with the overriding plate is not considered. We simulate the effect of the out-of-balance pressures with a velocity boundary condition (v_{retr}) applied at the model slab end in the slab-normal direction (Fig. 2c). This boundary condition takes into account the effect of both the slab-normal pressure difference along the model slab and that along the deeper part of the slab that is not physically included in the model.

We expect that the dip angle of long slabs cannot easily change. Therefore, to simulate long slabs we locally fix the dip angle of the model slab end. In the case of a short slab or a slab of limited along-strike extent, mantle material may flow more easily around the slab, thereby reducing dynamic pressure differences and allowing for a change in dip angle. In these cases, therefore, the dip angle of the slab is free to change dynamically.

3 MODELLING ANALYSIS

3.1 Model 1

We first simulate a relatively simple subduction situation (without slab retreat or advance). The subducting slab experiences an effective pull force F^0_{eff} (formed by force increments ΔF^0), oriented along the dip of the slab. The velocity of the right edge of the subducting plate at the surface is -4 cm yr^{-1} (v_{sub} in Fig. 2c). The minus sign indicates velocity directed towards the left. The overall rate of convergence between both side boundaries of the model is 4 cm yr^{-1}. Values of modelling parameters that are the same for all models are given in Table 1. Fig. 3 shows the results of model 1 (see also Table 2). The vertical displacement and horizontal velocity (averaged over 0.1 Myr) of the surface are shown at the top of the figure. The displacement is given relative to the surface of the initial model. During the evolution of the model the dip angle of the subducting plate remains near 45°, although it is allowed to change dynamically. The margin of the overriding plate is deflected downwards. The maximum subsidence is nearly 4 km after 2 Myr. The subducting slab is in tension due to the exerted pull, while the surface plates are both in compression.

Table 1. Modelling parameters.

Parameter	Value
Effective plate thickness	25 km
Young's modulus	5×10^{10} Pa
Poisson's ratio	0.25
Gravitational acceleration	9.80 m s^{-2}
Viscosity weak zone	5×10^{21} Pa s

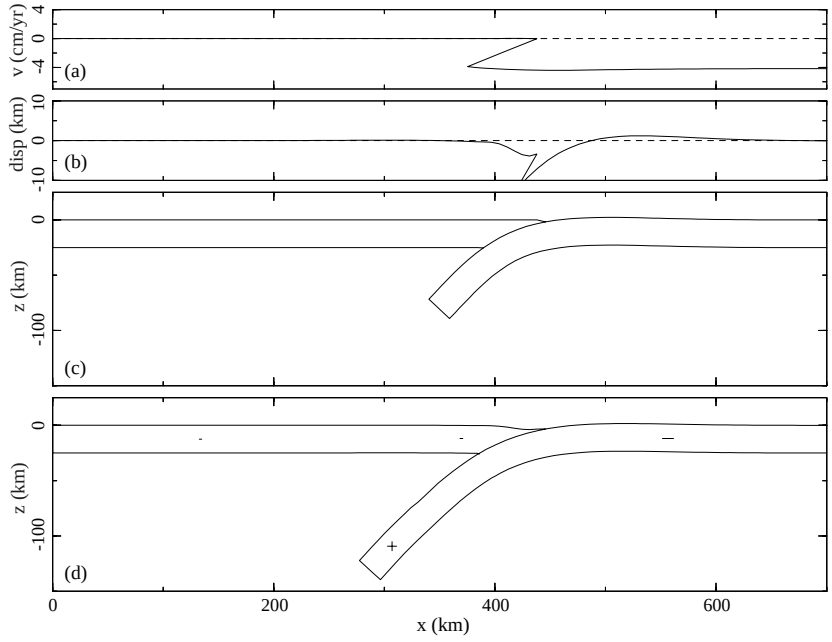

Figure 3. Model 1 (see also Table 2). Subduction of a negatively buoyant plate pushed at its right hand side by -4 cm yr^{-1}. In this and subsequent figures the subducting plate extends further to the right than shown here (initial model ends at 1226 km). Results are shown after 2 Myr. (a) Horizontal surface velocity averaged over last 0.1 Myr [positive (negative) velocity indicates motion to the right (left)]. (b) Total vertical surface displacement (relative to surface of initial model). (c) Initial model. (d) Model after 2 Myr, $+/-$ signs indicate in-plane tension/compression, respectively.

Table 2. Classification of models.

Model	$\times \Delta F^{0(1)}$	v_{retr} (cm yr^{-1})	Dip[2]	v_{sub} (cm yr^{-1})	v_{ovr} (cm yr^{-1})	$v^{(3)}_{conv}$ (cm yr^{-1})	μ	P_a shift (km)	Weak zone	Trench[4]	Figure
1	1	0	free	−4	0	4	0	0	n	n	3, 4
2	1.5	0	free	−4	0	4	0	0	n	n	5
3	0.5	0	free	−4	0	4	0	0	n	n	5
4	0	0	free	−4	0	4	0	0	n	n	5
5	0	0	free	−4	0	4	0	40	n	n	–
6	1	0	free	−4	2	6	0	0	n	r	6
7	1	0	free	−4	−2	2	0	0	n	f	–
8	1	2	fix	−4	0	4+	0	0	y	r	7
9	1	2	free	−4	0	4+	0	0	y	r	7
10	1	2	free	−4	0	4+	0	−20	y	r	7
11	1	2	fix	0	0	0+	0	0	y	r	8, 9
12	1	2	free	0	0	0+	0	0	y	r	–
13	1	0	free	−4	0	4	0.1	0	n	n	–
14	1	2	free	−4	0	4+	0.05	0	y	r	–

[1] Oriented along dip of slab.
[2] Dip angle of model slab end is either free or held fixed.
[3] Measured between the model left and right side boundaries. In the case of roll-back with back-arc extension, the local convergence rate across the plate boundary will be higher; this is indicated with a +.
[4] n: non-migrating; r: retreat; f: forward.

The evolution of vertical surface displacement is shown in Fig. 4. With time the overriding plate margin is deflected downwards until it has a maximum subsidence. The height of the flexural bulge of the subducting plate also achieves a maximum after approximately 2 Myr, after which it decreases slightly. Overall, there are no large changes in surface topography after 2 Myr (or 80 km of convergence). At this time the effects of initial conditions have disappeared and an equilibrium topography is reached (see also Section 2.3). In comparing surface displacements between different models we will use these equilibrium results.

The observation that vertical surface displacement and slab dip do not change much with time indicates that the velocity $\bar{v}_{sub}$ of the subducting plate at the surface and the pull force F^0_{eff} are in equilibrium with each other for the elastic rheology that is used. In model 1 the magnitude of the subduction velocity was 4 cm yr^{-1}. For higher or lower velocities equilibrium is maintained. For the same amount of plate convergence, surface topography is the same. This is in agreement with Toth & Gurnis (1998). These authors use a viscoelastic model that includes the asthenosphere and find that the topography of the plate margins is not substantially influenced by subduction being fast or slow. Therefore, we will not vary the magnitude of v_{sub} and we use 4 cm yr^{-1} in the following models.

The surface topography of our model 1 differs from the results of Gurnis *et al.* (1996) in that we do not find an uplift of the order of 1 to 2 km of the edge of the overriding plate margin next to the subduction fault. Toth & Gurnis (1998) show that this uplift reduces with a reduction in upper mantle viscosity. The inviscid asthenosphere in our model could, therefore, explain part of the topographic difference. Another contribution may be from (small) differences in numerical implementation of the subduction fault between the models.

In the next sections we report the effects of parameter variations with respect to model 1. Changes in driving force, velocity of the overriding plate, slab-normal pressures and friction along the subduction fault are examined.

3.2 Variation in slab buoyancy

We expect that changes in buoyancy of the subducting plate will affect vertical surface displacements significantly. We study

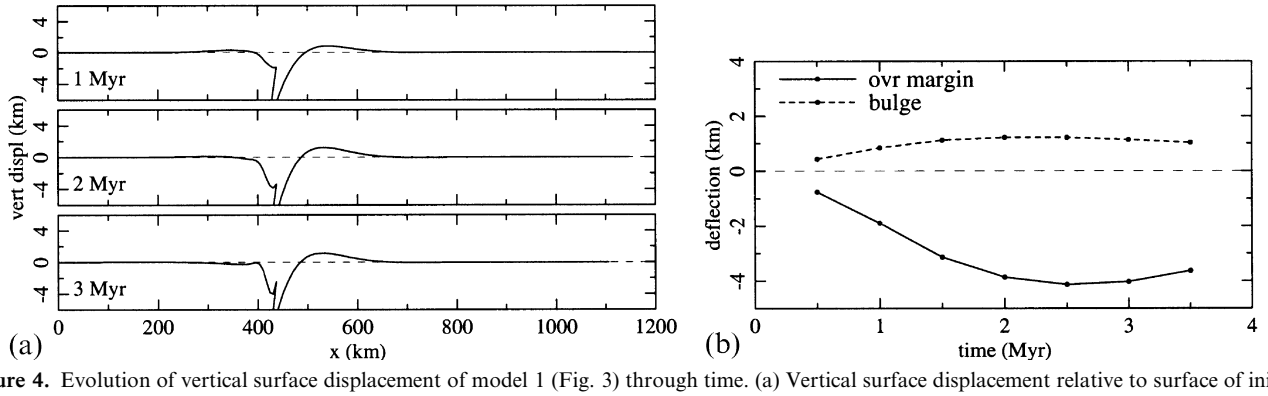

Figure 4. Evolution of vertical surface displacement of model 1 (Fig. 3) through time. (a) Vertical surface displacement relative to surface of initial model at three stages during model evolution (after 1, 2 and 3 Myr). Vertical scale is exaggerated 16 times. (b) Maximum downward deflection of overriding plate margin and maximum upward deflection of subducting plate (bulge) versus time. Small circles denote times for which values have been calculated.

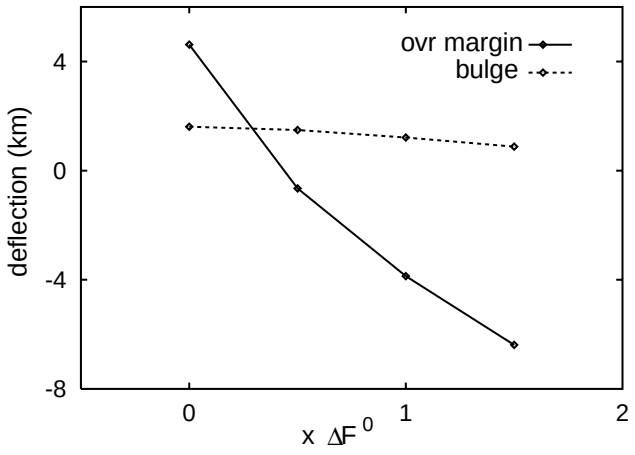

Figure 5. Effect of change in force increment ΔF on vertical surface displacement of two points located on the overriding and subducting plates (initially -7 and 173 km from the trench, respectively). Displacements are measured relative to the surface of the initial model after 80 km of convergence. See also models 1–4 in Table 2.

these effects by varying the force increment ΔF. Variations in ΔF may result from changes in the density difference between slab and mantle or from changes in viscous resistance to subduction. Fig. 5 shows the variation with ΔF of vertical surface displacement for points on the overriding and subducting plates. The range examined extends from $1.5 \times \Delta F^0$ (model 2), through ΔF^0 (model 1) and $0.5 \times \Delta F^0$ (model 3) to $\Delta F = 0$ (model 4). Displacements are evaluated after 80 km of convergence. There is a clear trend of increasing uplift of the overriding plate margin with decreasing ΔF (increasing buoyancy). An increase in ΔF (decrease in buoyancy) deepens the deflection of the margin of the overriding plate (to -6 km for model 2). In the range examined, the bulge height decreases by almost 1 km with increasing ΔF.

The development of vertical surface displacements is sensitive to the location of P_a. This parameter defines the top of the depth interval in which hydrostatic pressures across the slab are in balance (Fig. 2c). Pressure differences in the mantle or a change in density of the overriding plate, for example, may change the location of P_a. A shift in the oceanward direction in P_a of 40 km lowers the uplift of the overriding plate margin of model 4 ($\Delta F = 0$) by nearly 4.5 km (model 5, Table 2). In the following simulations P_a is kept at the same location as in model 1 so resulting surface displacements can be compared between the models.

3.3 Trench migration

3.3.1 Trench retreat and advance forced by the overriding plate

The location of a subduction zone trench is not necessarily stationary as is evidenced by observed migrations of trenches in the direction perpendicular to their strike. We first examine the surface effects of trench retreat (e.g. South America; Chase 1978; Gripp & Gordon 1990) and advance (e.g. Makran, Himalayas; Chase 1978; Royden 1993) forced by the motion of the overriding plate. The trench displacements are examined in an absolute reference frame. To simulate forced trench retreat a velocity v_{ovr} of 2 cm yr^{-1} is imposed at the left side of the model. Fig. 6 shows that after 80 km of convergence (after 1.35 Myr) the surface displacement for model 6 is the same as for model 1. In fact, the models are very similar, since the convergence obtained by moving both the overriding and subducting side boundaries can equally well be simulated by keeping the overriding plate fixed laterally and moving only the subducting plate. This also applies to the case of trench advance (model 7, not shown).

In models 6 and 7 the subducted slab is free to migrate laterally with respect to the mantle in response to the imposed surface velocities. It may, however, be possible that the slab feels a resistance to lateral migration through the mantle, for example, due to increased mantle pressures in the direction of slab translation. Active overriding by a continent may then lead to a low dip angle at shallow depths followed by a steeper slab further down, similar to what is observed along parts of the South American subduction zone (Barazangi & Isacks 1979; Cahill & Isacks 1992). Model 6b again simulates trench retreat forced by the overriding plate, only in this case it is assumed that the deeper part of the slab cannot migrate laterally. Therefore, movement of the model slab end is constrained to the along-dip direction. Since retrograde motion of the slab

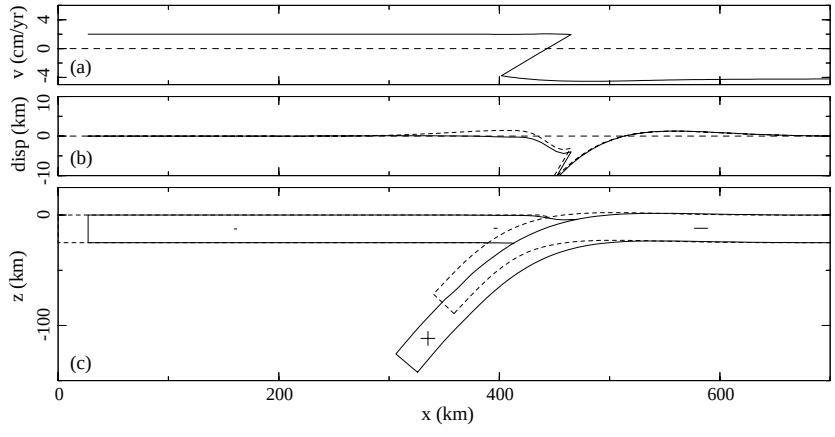

Figure 6. Model 6. Subduction zone roll-back forced by an advancing overriding plate. The velocity of the subducting plate is -4 cm yr^{-1} and the overriding plate moves at 2 cm yr^{-1}. Results are shown after 80 km convergence (after 1.35 Myr). (a) Horizontal surface velocity averaged over last 0.1 Myr. (b) Vertical surface displacement; dotted line is displacement for model 6b (see text). (c) Model configuration; dotted line is outline of initial model; $+/-$ signs indicate in-plane tension/compression, respectively.

is prevented from relatively shallow depths downwards, this can be considered as an end-member situation. Uplift of the overriding plate margin is induced that reaches a maximum magnitude of nearly 1.5 km after 80 km of convergence (Fig. 6b). With respect to models 1 and 6, the overriding plate experiences an increase in in-plane compression.

3.3.2 *Roll-back caused by negative buoyancy of the slab*

When the slab-normal component of slab pull is not completely balanced by dynamic mantle pressures, the subducting plate displays a tendency towards roll-back. Subduction zone roll-back can only occur if the overriding plate allows it. Either the overriding plate must be able to follow the retreat of the subducting plate or it must be able to extend. In the latter case a back-arc basin develops. We allow for subduction zone retreat through the introduction of a 100 km long weak zone with a lower viscosity (5×10^{21} Pa s) in the overriding plate. This part of the model has a Newtonian viscoelastic rheology, while the rest of the model remains elastic.

Model 8 simulates subduction zone retreat for a long slab. We assume that in this case the deeper part of the subducting slab will impede changes in dip angle. Therefore, we locally fix the dip angle of the model slab end. The magnitude of the slab-normal velocity at the model slab end is 2 cm yr^{-1} and $v_{\rm sub}$ is -4 cm yr^{-1}. After 80 km of convergence (after 1.05 Myr) the trench has retreated by around 39 km. At this time, the subsidence of the overriding plate margin is nearly 4 km at maximum, while in the back-arc area a basin has developed (Fig. 7a).

In the case of a short subducting slab, dynamic pressure differences across the slab may be reduced by the flow of mantle material around the slab end. The dip angle of the slab may then change during subduction. For model 9 the dip angle of the model slab end increases by around 13° in 1 Myr. The steepening of the slab is accompanied by an increase in the velocity of retreat. Overall, the average velocity of roll-back is lower than for model 8. In 1.35 Myr (80 km of convergence) the trench retreats by 24 km. The maximum subsidence of the overriding plate is 6.4 km (Fig. 7b).

The subsidence of the overriding plate margin may be reduced by a change in the pressure-balance parameter $P_{\rm a}$. For the case of non-migrating subduction we have shown that an oceanward shift in $P_{\rm a}$ lowers surface uplift. In a similar manner a shift towards the continent reduces subsidence of the overriding plate margin, as is shown in Fig. 7(c) (model 10). A continentward shift may, for example, be caused by a lower density of the overriding plate lithosphere.

3.3.3 *Roll-back in a land-locked basin setting*

A land-locked basin (Le Pichon 1982) refers to an oceanic basin trapped within a continental collision zone. In this case subduction of the basin can be achieved through roll-back of the trench and extension of the overriding plate. Model 11 simulates a land-locked basin setting. Neither side boundary of the model is allowed to move laterally ($v_{\rm sub} = v_{\rm ovr} = 0$ cm yr^{-1}). The slab-parallel driving force is again $F^0_{\rm eff}$, while the slab-normal velocity at the model slab end is 2 cm yr^{-1}. We assume a long subducting slab, therefore the dip angle of the model slab end is held fixed. Fig. 8 shows the results of model 11 after 2.6 Myr. The amount of trench retreat is 83 km. The average rate of roll-back is, therefore, around 3.2 cm yr^{-1}. The velocity of the overriding plate margin depends strongly on the magnitude of the slab-normal velocity $v_{\rm retr}$. For example, for a slab-normal velocity of 1 cm yr^{-1} the average rate of roll-back is 1.6 cm yr^{-1}. The velocity of roll-back is to a lesser extent sensitive to the value of the viscosity of the weak zone. A low viscosity value facilitates roll-back. In the case of high viscosity, the subducting plate is held back by the strong overriding lithosphere. In the latter situation the overriding plate margin will deepen as it is partly dragged along by the sinking subducting plate. We find that the surface topography after 80 km of convergence is the same for models in which the values for the viscosity of the weak zone and $v_{\rm retr}$ are inversely linearly related. This is due to the Maxwell viscoelastic behaviour of the weak zone.

If the dip angle of the subducting plate is allowed to change during roll-back, the slab steepens by 16° in 4 Myr (model 12, not shown separately). The average velocity of roll-back is lower in comparison with model 11 and amounts to 2.1 cm yr^{-1} after 3.6 Myr. The maximum subsidence of the overriding plate margin is increased by around 1.5 km.

Extension in the overriding plate localizes in the weak zone. A small amount of flank uplift and deepening of the basin adjacent to the flanks can be observed (Figs 7 and 8). The uplift/deepening pair is probably caused by the variation in plate thickness across the boundary of the basin. This results in a change in the depth of the horizontal force, creating a moment that bends the plate (Morgan *et al.* 1987). Tension in

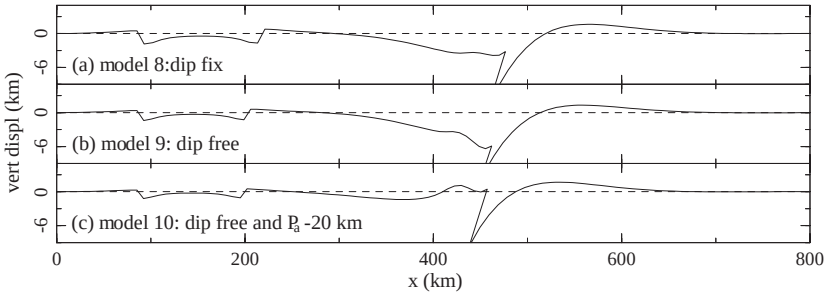

Figure 7. Vertical surface displacements for models in which the subducting slab retreats due to its negative buoyancy. Displacements are relative to the surface of the initial model and are measured after 80 km of convergence. The viscosity of the weak zone in the overriding plate is 5×10^{21} Pa s. $v_{\rm retr} = 2$ cm yr^{-1} and $v_{\rm sub} = -4$ cm yr^{-1}. (a) Model 8. Dip of model slab end held fixed ('long slab'). (b) Model 9. Dip of model slab end free ('short slab'). (c) Model 10. Dip free and $P_{\rm a} - 20$ km. Vertical scale is exaggerated 6 times.

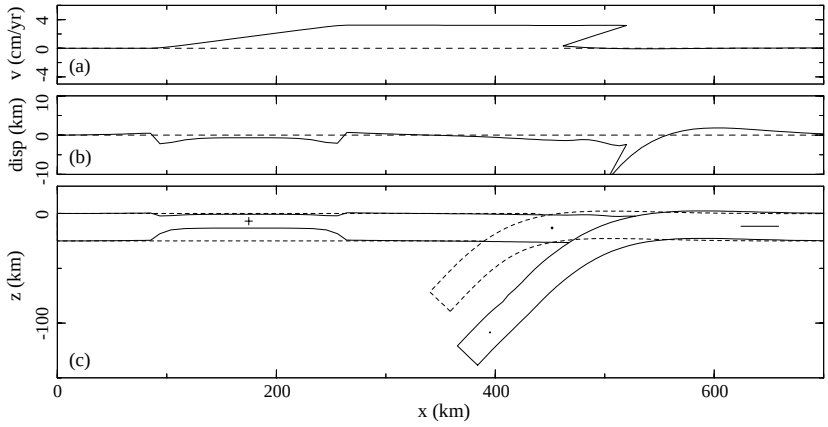

Figure 8. Model 11. Subduction zone roll-back in a land-locked basin setting. The side boundaries of the surface plates are fixed laterally. Viscosity of the weak zone in the overriding plate is 5×10^{21} Pa s and $v_{retr} = 2$ cm yr^{-1}. Results are shown after 80 km of convergence (after 2.6 Myr). Panels as in Fig. 6.

the overriding plate is shown in Fig. 9. The small deviation of tension from the horizontal near the boundaries of the weak zone is in agreement with the postulated bending moments across these boundaries.

3.4 Friction

Friction along the interplate contact increases the resistance to subduction. In model 13 an average coefficient of friction of $\mu = 0.1$ is imposed on the subduction fault (model not shown separately). In all other aspects the model is the same as model 1. The friction leads to a deepening of the overriding plate margin. Relative to model 1 the extra subsidence is more than 1 km after 2 Myr. This result is in qualitative agreement with the results of Cattin *et al.* (1997), who report a deepening of the trench with higher values for the friction coefficient. Hassani *et al.* (1997) show that stresses in the overriding plate reverse from tension to compression with an increasing coefficient of friction. In their model slab pull acts vertically, while slab dip increases during model evolution. Since in model 1 the effective pull force is directed along dip of the slab, the overriding plate is already in compression for $\mu = 0$. When we include slab-normal forcing (through v_{retr}) and allow for dip angle changes we also find a reversal in sign (from tension to compression) of deviatoric stresses in the overriding plate with increasing friction.

Model 14 is the same as roll-back model 9 except for an average coefficient of friction of $\mu = 0.05$ on the subduction fault. Relative to model 9, tension in the back-arc area is reduced, while the velocity of trench retreat reduces. Subsidence of the overriding plate margin after 80 km of convergence increases by nearly 2.5 km. The increase in compression and reduction of trench retreat with increasing friction on the subduction fault are caused by the stronger coupling of the subducting to the overriding plate. The extreme end-member would be the case in which the plates are fully coupled (i.e. locked contact) and no differential displacement occurs along the subduction fault. The horizontal velocity of the subducting plate ($\bar{v}_{sub}$) would then induce a large compression in both surface plates.

3.5 Vertical motions induced by variations in a subduction zone system

Changes in a subduction zone system are reflected in horizontal and vertical surface displacements. The results we have obtained show that vertical surface displacements at a convergent plate margin are sensitive to the buoyancy of the subducting material, friction on the subduction fault, retrograde motion of the slab and resistance to changes in dip angle. By comparing topographic profiles we can predict the effects that changes in subduction zone parameters will have. To this end Fig. 10 shows vertical surface displacements relative to the surface of model 1. The topography of the models is compared after the same amount of convergence of 80 km. For model 1 this is obtained after 2 Myr. The topographic profiles are aligned to the same trench position before the profile of model 1 is subtracted. These are surface displacements that would be induced if the subduction of model 1 were changed with respect to one of the examined parameters. The maximum surface displacement varies between approximately -6 and

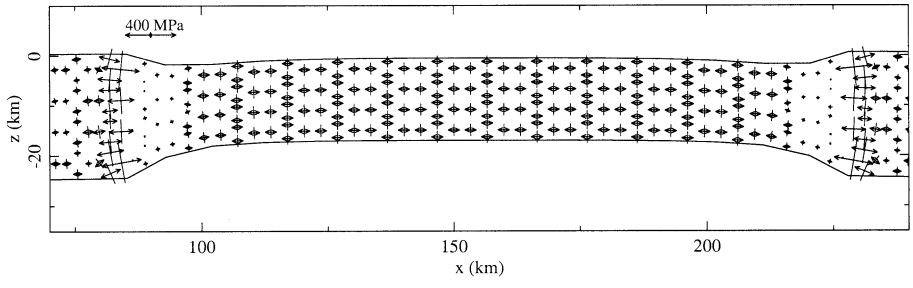

Figure 9. Deviatoric stresses in the back-arc region for subduction zone roll-back of model 11 (Fig. 8) after 1.5 Myr.

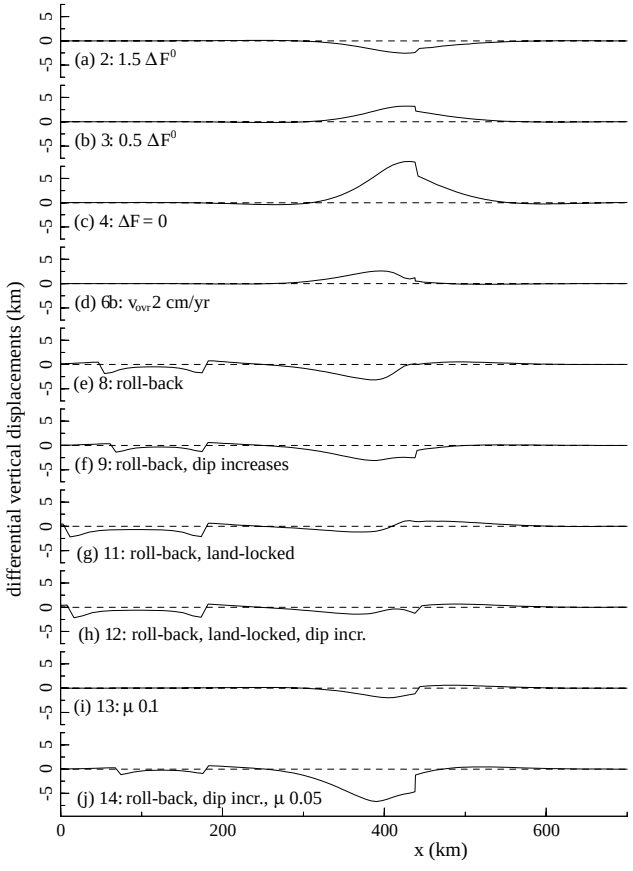

Figure 10. Differential vertical surface displacements resulting from changes in the subduction zone parameters. Displacements are relative to model 1 (Fig. 3) after 80 km of convergence. Trench positions have been aligned before subtraction. Vertical scale is exaggerated 6 times. (a) Increase in ΔF, (b) decrease in ΔF, (c) $\Delta F = 0$, (d) $v_{ovr} = 2$ cm yr^{-1} with resistance to lateral migration of deeper part of the slab, (e) roll-back with dip of model slab end fixed, (f) roll-back with dip free, (g) roll-back in land-locked basin setting with dip of model slab end fixed, (h) roll-back in land-locked basin setting with dip free, (i) friction along the subduction fault, and (j) roll-back with friction along the subduction fault and dip free. Values of relevant parameters and model numbers are shown in the lower left corner of the panels.

8 km. In all cases the displacements are largest near the plate margins. On average a region of around 200 km is affected. The lateral extent of this region is, however, determined by our choice for the effective elastic thickness of the lithospheric plates.

Our results show that an increase in the pull force increment ΔF (decrease in buoyancy) leads to subsidence of both plate margins (Fig. 10a). A decrease in pull force (increase in buoyancy) leads to uplift (Figs 10b and c). These findings agree with previous studies (Hassani *et al.* 1997; Toth & Gurnis 1998). A change in motion of the overriding plate with respect to the reference model leads to trench migration. When the motion of the overriding plate changes from zero to advancing, uplift of the overriding plate margin is induced only when retrograde motion of the deeper part of the subducted slab is prevented (Fig. 10d). Figs 10(e) and (f) show that subsidence of the overriding plate margin may be expected in the case of subduction zone retreat caused by the negative buoyancy of the slab. This can also be seen in the results of Hassani *et al.* (1997). Subsidence of the overriding plate margin is (more than half) less for models of subduction zone roll-back in a land-locked basin setting than for models in which the retrograde motion is superposed on the 'normal' (non-migrating) subduction (Figs 10g and h). Extension in the back-arc area leads to the development of a basin (Figs 10e–h). Friction on the subduction fault will induce subsidence of the overriding plate margin (Figs 10i and j).

4 DISCUSSION

4.1 Trench retreat

Our results indicate that different driving mechanisms for trench retreat may have different expressions in vertical surface displacement of the overriding plate margin. For trench retreat forced by the motion of the overriding plate we expect higher topography than for the case of trench retreat due to the negative buoyancy of the slab. This signal would be superimposed on the topographic expressions of other processes active near a convergent plate margin, for example, magmatism and underplating. An example of trench retreat forced by the motion of the overriding plate may be found along the west coast of South America, where South America moves towards the subducting Nazca plate (Chase 1978). Naturally, a component of retreat may still be due to the negative buoyancy of the subducting plate. The average elevation of the Central Andes is near 4 km (Froidevaux & Isacks 1984). The back-arc region is characterized by a compressional stress regime (Uyeda & Kanamori 1979; Froidevaux & Isacks 1984). Models 6 and 6b (Fig. 6) describe continuing subduction with a component of slab roll-back, which is caused by the motion of the overriding plate. In both cases the overriding plate is in compression. Compression is higher when retrograde motion of the deeper part of the slab is restricted (model 6b). Note that the amount of trench retreat will be reduced when significant tectonic erosion occurs (Lallemand 1995). Large compression in the overriding plate may also be induced by stronger coupling of the two plates along the subduction contact (models 13 and 14). Significant coupling, at least at seismogenic scales, is indicated by the large thrust earthquakes at the Chilean margin (Uyeda & Kanamori 1979). We find that increased coupling (imposed by larger friction on the subduction fault) slows subduction while reducing the amount of trench retreat. Also, a component of subsidence is added to the overriding plate margin. The observations of continuing subduction and a high topography of the overriding plate margin in the Andes may indicate that very strong coupling is less likely on geological timescales.

Examples of trench retreat due to sinking of the subducting slab under its own negative buoyancy are the Mariana arc (e.g. Molnar & Atwater 1978), the Apennines (Italy) (e.g. Malinverno & Ryan 1986) and the Aegean region (e.g. Le Pichon 1982). All are characterized by extensional back-arc basins.

4.2 Model aspects

In this section we further discuss some aspects, e.g. boundary conditions, of our numerical modelling procedure.

It is assumed that in the depth interval below P_a (Fig. 2c), pressure increments due to the hydrostatic pressure cancel each other across the subducted slab. Models 5 and 10 show that

vertical surface displacements are sensitive to the choice of this parameter. P_a is defined by the (perpendicular downward projection of the) point of contact of the overriding plate with the subducting plate at the surface. The location of P_a may be affected by the density of the overriding plate, the presence of a large accretionary wedge at the surface and pressure differences in the asthenosphere near the corner region. As shown by models 5 and 10, the formation of rather large surface displacements (e.g. Fig. 10c) may be prevented by shifting P_a. We preferred to define P_a in the same manner for the models of Fig. 10 and not to define arbitrary shifts between the models.

The insensitivity of the model to variations in surface velocity can be explained by the partitioning of factors that drive deformation in a pull force acting on the slab and velocities at the surface side boundaries of the plates. In this way the slab is free to adjust immediately to changes in the system, for example, a higher convergence velocity at the surface leads to a higher velocity of the slab. It is to be expected that changes in topography will result if the slab needs a long time to react to changes (i.e. is relatively inert). As illustrated by model 6b, for example, trench retreat forced by the overriding plate motion would then induce uplift of the overriding plate margin. Similarly, it could be expected that a change in slab buoyancy may lead to a change in the velocity of the subducting plate at the surface as the system seeks a new equilibrium. In models 2, 3 and 4 we assume that such an adjustment does not occur and is, for example, prevented by the interaction with other lithospheric plates.

In our quantification of vertical displacements, the effects of erosion and sedimentation have not been included. Sedimentation would lead to further subsidence, whereas the calculated subsidence for some of the models is already quite large. As mentioned above, pressure differences in the mantle, for example, may act to reduce surface displacements. The effect of gravity within the plates has also been neglected in the models. Therefore, gravitational spreading of topographic highs, which will reduce surface uplift, is not taken into account.

In our model formulation we assume that a shallow slab dip may result from dynamic equilibrium between slab and upper mantle, in contrast with Becker *et al.* (1999). We do agree with these authors that other processes such as, for example, anchoring of the slab at the transition zone between upper and lower mantle or background mantle flow (Doglioni 1993, 1994; Olbertz *et al.* 1997) may contribute to maintaining a lower slab dip. Such processes were not included in our analysis.

5 CONCLUSIONS

We have shown that significant vertical surface displacements at convergent plate margins may occur during ongoing subduction. We have quantified these displacements using a 2-D model in which the plates have an effective elastic thickness. Viscoelastic deformation is allowed to occur in the back-arc region in some instances of slab retrograde motion. The model is used to study the surface effects of subduction zone dynamics on a timescale of a few million years. We conclude that vertical surface displacements induced by changes in a subduction system can reach a magnitude of a few (around 2–4) kilometres on the margins of both the overriding and the subducting plates. The displacements are sensitive to slab buoyancy, friction along the subduction fault, retrograde motion of the slab and (resistance to) changes in dip angle. A decrease in the buoyancy of the subducting material leads to a deepening of the plate margins, while an increase in buoyancy leads to uplift. An increase in friction along the subduction fault deepens the overriding plate margin. Retrograde motion of the slab caused by the negative buoyancy of the subducting lithosphere induces subsidence of the overriding plate margin. This subsidence is less pronounced when roll-back occurs in a land-locked basin setting. We expect that variations in velocity of the surface plates will induce vertical surface displacements if the subducted slab cannot easily adjust to these velocity changes.

Trench retreat forced by the motion of the overriding plate is characterized by higher topography on the overriding plate margin than the case of retreat due to sinking of the negatively buoyant slab. In-plane stress in the back-arc region is compressive for trench retreat due to the overriding plate motion and tensional for trench retreat (roll-back) due to sinking of the slab. Our results confirm the findings of Hassani *et al.* (1997) that an increase in interplate friction can change tension in the overriding plate to compression.

ACKNOWLEDGMENTS

We thank P. Th. Meijer for discussions on the Andes. M. Gurnis and an anonymous reviewer are thanked for their helpful reviews. This work was conducted under the programme of the Vening Meinesz Research School of Geodynamics. During the investigations reported here SB was financially supported by the Geosciences Foundation (GOA/ALW) of the Netherlands Organisation for Scientific Research (NWO).

REFERENCES

Audley-Charles, M.G., 1986. Rates of Neogene and Quaternary tectonic movements in the Southern Banda Arc based on micropalaeontology, *J. geol. Soc. Lond.,* **143,** 161–175.

Barazangi, M. & Isacks, B.L., 1979. Subduction of the Nazca plate beneath Peru: evidence from spatial distribution of earthquakes, *Geophys. J. R. astr. Soc.,* **57,** 537–555.

Becker, T.W., Faccenna, C., O'Connell, R.J. & Giardini, D., 1999. The development of slabs in the upper mantle: Insights from numerical and laboratory experiments, *J. Geophys. Res.,* **104,** 15 207–15 226.

Cahill, T. & Isacks, B.L., 1992. Seismicity and shape of the subducted Nazca plate, *J. geophys. Res.,* **97,** 17 503–17 529.

Caldwell, J.G., Haxby, W.F., Karig, D.E. & Turcotte, D.L., 1976. On the applicability of a universal elastic trench profile, *Earth planet. Sci. Lett.,* **21,** 239–246.

Cattin, R., Lyon-Caen, H. & Chéry, J., 1997. Quantification of interplate coupling in subduction zones and forearc topography, *Geophys. Res. Lett.,* **24,** 1563–1566.

Chapple, W.M. & Forsyth, D.W., 1979. Earthquakes and bending of plates at trenches, *J. geophys. Res.,* **84,** 6729–6749.

Chase, C.G., 1978. Extension behind island arcs and motions relative to hot spots, *J. geophys. Res.,* **83,** 5385–5387.

Chatelain, J., Molnar, P., Prévot, R. & Isacks, B., 1992. Detachment of part of the downgoing slab and uplift of the New Hebrides (Vanuatu) islands, *Geophys. Res. Lett.,* **19,** 1507–1510.

Christensen, U.R., 1996. The influence of trench migration on slab penetration into the lower mantle, *Earth planet. Sci. Lett.,* **140,** 27–39.

Conrad, C.P. & Hager, B.H., 1999. Effects of plate bending and fault strength at subduction zones on plate dynamics, *J. geophys. Res.,* **104,** 17 551–17 571.

Cross, T.A. & Pilger, R.H., Jr., 1982. Controls of subduction geometry, location of magmatic arcs, and tectonics of arc and back-arc regions, *Geol. Soc. Am. Bull.,* **93,** 545–562.

Davies, G.F., 1995. Penetration of plates and plumes through the mantle transition zone, *Earth planet. Sci. Lett.,* 507–516.
Doglioni, C., 1993. Some remarks on the origin of foredeeps, *Tectonophysics,* **228,** 1–20.
Doglioni, C., 1994. Foredeeps versus subduction zones, *Geology,* **22,** 271–274.
Dvorkin, J., Nur, A., Mavko, G. & Ben-Avraham, Z., 1993. Narrow subducting slabs and the origin of backarc basins, *Tectonophysics,* **227,** 63–79.
Dziewonski, A.M. & Anderson, D.L., 1981. Preliminary reference Earth model, *Phys. Earth planet. Inter.,* **25,** 297–356.
Elsasser, W.M., 1971. Sea-floor spreading as thermal convection, *J. geophys. Res.,* **76,** 1101–1112.
Froidevaux, C. & Isacks, B.L., 1984. The mechanical state of the lithosphere in the Altiplano-Puna segment of the Andes, *Earth planet. Sci. Lett.,* **71,** 305–314.
Giunchi, C., Sabadini, R., Boschi, E. & Gasperini, P., 1996. Dynamic models of subduction: geophysical and geological evidence in the Tyrrhenian Sea, *Geophys. J. Int.,* **126,** 555–578.
Gripp, A.E. & Gordon, R.G., 1990. Current plate velocities relative to the hotspots incorporating the Nuvel-1 global plate motion model, *Geophys. Res. Lett.,* **17,** 1109–1112.
Gurnis, M., 1992. Rapid continental subsidence following the initiation and evolution of subduction, *Science,* **255,** 1556–1558.
Gurnis, M., Eloy, C. & Zhong, S., 1996. Free-surface formulation of mantle convection—II. Implication for subduction-zone observables, *Geophys. J. Int.,* **127,** 719–727.
Hassani, R., Jongmans, D. & Chéry, J., 1997. Study of plate deformation and stress in subduction processes using two-dimensional models, *J. geophys. Res.,* **102,** 17 951–17 965.
Lallemand, S., 1995. High rates of arc consumption by subduction processes: some consequences, *Geology,* **23,** 551–554.
Le Pichon, X., 1982. Land-locked oceanic basins and continental collision: the Eastern Mediterranean as a case example, in *Mountain Building Processes,* pp. 201–211, ed. Hsü, K.J., Academic Press, London.
Lundberg, N. & Dorsey, R.J., 1988. Synorogenic sedimentation and subsidence in a Plio-Pleistocene collisional basin, Eastern Taiwan, in *New Perspectives in Basin Analysis,* pp. 265–280, eds Kleinspehn, K.L. & Paola, C., Springer-Verlag, New-York.
Malinverno, A. & Ryan, W.B.F., 1986. Extension in the Tyrrhenian Sea and shortening in the Apennines as result of arc migration driven by sinking of the lithosphere, *Tectonics,* **5,** 227–245.
Marton, F.C., Bina, C.R., Stein, S. & Rubie, D.C., 1999. Effects of slab mineralogy on subduction rates, *Geophys. Res. Lett.,* **26,** 119–122.
Melosh, H.J. & Raefsky, A., 1980. The dynamical origin of subduction zone topography, *Geophys. J. R. astr. Soc.,* **60,** 333–354.
Melosh, H.J. & Raefsky, A., 1983. Anelastic response of the earth to dip slip earthquakes, *J. geophys. Res.,* **88,** 515–526.
Melosh, H.J. & Williams, C.A., Jr., 1989. Mechanics of graben formation in crustal rocks: a finite element analysis, *J. geophys. Res.,* **94,** 13 961–13 973.
Molnar, P. & Atwater, T., 1978. Interarc spreading and Cordilleran tectonics as alternatives related to the age of subducted oceanic lithosphere, *Earth planet. Sci. Lett.,* **41,** 330–340.
Morgan, J.P., Parmentier, E.M. & Lin, J., 1987. Mechanisms for the origin of mid-ocean ridge axial topography: implications for the thermal and mechanical structure of accreting plate boundaries, *J. geophys. Res.,* **92,** 12 823–12 836.
Negredo, A.M., Sabadini, R. & Giunchi, C., 1997. Interplay between subduction and continental convergence: a three-dimensional dynamic model for the Central Mediterranean, *Geophys. J. Int.,* **131,** F9–F13.
Olbertz, D., Wortel, M.J.R. & Hansen, U., 1997. Trench migration and subduction zone geometry, *Geophys. Res. Lett.,* **24,** 221–224.
Royden, L.H., 1993. The tectonic expression slab pull at continental convergent boundaries, *Tectonics,* **12,** 303–325.
Shemenda, A.I., 1993. Subduction of the lithosphere and back arc dynamics: insights from physical modelling, *J. geophys. Res.,* **98,** 16 167–16 185.
Stevenson, D.J. & Turner, J.S., 1977. Angle of subduction, *Nature,* **270,** 334–336.
Toth, J. & Gurnis, M., 1998. Dynamics of subduction initiation at preexisting fault zones, *J. geophys. Res.,* **103,** 18 053–18 067.
Tovish, A., Schubert, G. & Luyendyk, B.P., 1978. Mantle flow pressure and the angle of subduction: non-newtonian corner flows, *J. geophys. Res.,* **83,** 5892–5898.
Uyeda, S. & Kanamori, H., 1979. Back-arc opening and the mode of subduction, *J. geophys. Res.,* **84,** 1049–1061.
Wallace, M.H. & Melosh, H.J., 1994. Buckling of a pervasively faulted lithosphere, *Pure appl. Geophys.,* **142,** 239–261.
Watts, A.B. & Talwani, M., 1974. Gravity anomalies seaward of deep-sea trenches and their tectonic implications, *Geophys. J. R. astr. Soc.,* **36,** 57–90.
Westaway, R., 1993. Quaternary uplift of Southern Italy, *J. geophys. Res.,* **98,** 21 741–21 772.
Whittaker, A., Bott, M.H.P. & Waghorn, G.D., 1992. Stresses and plate boundary forces associated with subduction plate margins, *J. geophys. Res.,* **97,** 11 933–11 944.
Zhong, S. & Gurnis, M., 1994. Controls on trench topography from dynamic models of subducted slabs, *J. geophys. Res.,* **99,** 15 683–15 695.

APPENDIX A: SLAB PULL FORCE

We determine the magnitude of the effective pull force for our numerical model by measuring the force on the slab for a velocity-driven subduction model. For this particular case subduction is maintained through a velocity at the surface (v_{sub}) and an along-dip velocity at the model slab end of the same magnitude. Steady-state subduction (that is, slab dip and velocity remain the same with time) results for a model in which the measured pull force and v_{sub} are applied. Subduction of a new slab segment at the trench generates a force increment ΔF (Fig. 2b). This incremental force can be thought of as the force responsible for the acceleration of the segment of the subducting plate from a zero vertical velocity before the trench to the vertical (component of) subduction velocity at depth below the overriding plate. It is the force increment that we actually measure: $\Delta F^0 = 2.6 \times 10^8$ N m^{-1} per metre vertical sinking. We assume that the summation of these increments along the slab forms the effective pull force $F^0_{\rm eff} = 2.4 \times 10^{13}$ N m^{-1}. The slab pull force would, therefore, be equal to or higher than this value. As discussed in Section 2.4.3, we assume that once the slab has straightened out, the along-dip component of slab pull is balanced by viscous resistive forces. Therefore, the integration of the force increments is performed down to a depth of 150 km. In all models the force increment is applied in a shallow depth interval between 60 and 80 km. This forcing interval lies below the region of largest bending of the subducting plate and above the initial model slab end. We have verified that a larger interval or a vertical shift within the limits imposed by the size of the initial model does not affect surface displacements.